Spectro-polarimetric BRDF determination of objects using in-scene calibration materials for polarimetric imagers.

Brent Bartlett, Chabitha Devaraj, Michael Gartley, Carl Salvaggio, John R. Schott

Rochester Institute of Technology, Chester F. Carlson Center for Imaging Science, Digital Imaging and Remote Sensing Laboratory, Rochester, NY, USA

ABSTRACT

For sensing systems that characterize the spectro-polarimetric radiance reaching the camera, the origin of the sensed phenomenology is a complex mixture of sources. While some of these sources do not contribute to the polarimetric signature, many do such as the downwelled sky polarization, the target and background p-BRDF(polarimetric bi-directional reflectance distribution function), the upwelled sky polarization, and the camera Mueller matrix transfer function. In this paper we investigate candidate in-scene calibration materials potentially allowing for portions of the p-BRDF to be derived for material surfaces throughout the scene. Extraction of target p-BRDF from the sensed spectro-polarimetric energy may result in improved target detection performance in the future. Results using both synthetic and real data are presented.

Keywords: calibration, BRDF, polarimetric, measurement

1. INTRODUCTION

Many polarimetric applications in remote sensing rely on using models of the p-BRDF (polarimetric bi-directional reflectance distribution function) to describe the way in which light interacts with scene materials.[1] It is not clear however which model will perform with the highest accuracy with a particular material or scene geometry. Due to this situation it is desirable to devise a collection strategy which can provide empirical data allowing portions of the p-BRDF to be extracted for different materials across varying scene geometries. This can provide valuable inputs to the various p-BRDF models allowing for greater accuracy.

In particular, the downwelling radiance field can be highly linearly polarized and impart polarimetric signatures to the scene. A polarimetric panel cluster has been designed to allow for the calibration of spectro-polarimetric imaging systems. Using known reflectance values for diffuse materials present in the scene, both diffuse and specular portions of the p-BRDF can be retrieved for glossy materials within the same scene. The modeling environment of DIRSIG, in conjunction with MODTRAN-P, is used to model the collected scene and provide for additional input values required for the p-BRDF retrieval process. This process is demonstrated using both synthetic and real scene data.

2. BACKGROUND AND THEORY

The generalized version of the bidirectional reflectance distribution function can be expressed as a ratio of the irradiance incident onto a surface versus the radiance scattered off from the surface as shown in equation 1.

$$\mathbf{f}_{brdf} = \frac{dL(\theta_r, \phi_r; \lambda)}{dE(\theta_i, \phi_i; \lambda)} \tag{1}$$

This relationship can also be expressed in a polarimetric Stokes parameter representation as shown in equation 2 (note that the wavelength dependence is implicit in the rest of the derivation).

Further author information: E-mail: bdbpci@cis.rit.edu, Telephone: 1 585 475 5037

Polarization Science and Remote Sensing IV, edited by Joseph A. Shaw, J. Scott Tyo,
Proc. of SPIE Vol. 7461, 74610T · © 2009 SPIE · CCC code: 0277-786X/09/$18 · doi: 10.1117/12.825359

$$\begin{bmatrix} L_0 \\ L_1 \\ L_2 \\ L_3 \end{bmatrix}_{out} = \begin{bmatrix} f_{00} & f_{01} & f_{02} & f_{03} \\ f_{10} & f_{11} & f_{12} & f_{13} \\ f_{20} & f_{21} & f_{22} & f_{23} \\ f_{30} & f_{31} & f_{32} & f_{33} \end{bmatrix} \begin{bmatrix} E_0 \\ E_1 \\ E_2 \\ E_3 \end{bmatrix}_{in} \tag{2}$$

Characterizing the entire 4x4 representation for the p-BRDF can be quite challenging. However, in passive remote sensing it is often safe to assume that the contribution of circular polarization is negligible.[2] This assumption collapses the Stokes vector to three elements and equation 2 can be reduced to the following.

$$\begin{bmatrix} L_0 \\ L_1 \\ L_2 \end{bmatrix}_{out} = \begin{bmatrix} f_{00} & f_{01} & f_{02} \\ f_{10} & f_{11} & f_{12} \\ f_{20} & f_{21} & f_{22} \end{bmatrix} \begin{bmatrix} E_0 \\ E_1 \\ E_2 \end{bmatrix}_{in} \tag{3}$$

Finally, when considering a source that is only randomly polarized (such as the direct sun component, E_s) only the first column of equation 3 need be considered.

$$\begin{bmatrix} S_0 \\ S_1 \\ S_2 \end{bmatrix}_{out} = \begin{bmatrix} f_{00} \\ f_{10} \\ f_{20} \end{bmatrix} E_s \tag{4}$$

While these relationships can be used in a relatively straight forward manner when measuring the p-BRDF in the laboratory, they must be incorporated into a more complex governing equation when outside the laboratory. A method for exacting background polarimetric signatures utilizing the governing equation for outdoor measurements has been shown.[3] A similar formulation of the governing equation for sensor reaching radiance, not accounting for adjacency effects, can be expressed as the following where each component is a 3x1 stokes vector:

$$\vec{L}_s = \vec{L}_r + \vec{L}_d + \vec{L}_u \tag{5}$$

Each term in this equation contains a portion of the sensor reaching radiance which is shown in Figure 1 and which is more throughly explained in equations 6 - 8.

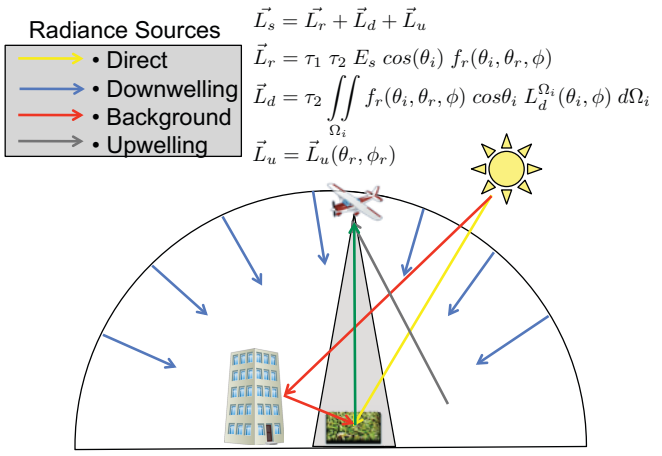

Figure 1. Diagram showing sources of sensor reaching radiance and their interactions with surface materials.

$$\vec{L}_r = \tau_1(\theta_i)\ \tau_2(\theta_r)\ E_s\ cos(\theta_i)\ \vec{f}_r(\theta_i, \theta_r, \Delta\phi) \tag{6}$$

where $\vec{L}_r$ is the reflected direct solar radiance, τ_1 is the atmospheric transmission along the sun target path, τ_2 is the atmospheric transmission along the target sensor path, E_s is the exoatmospheric irradiance, θ_i is the solar

zenith angle, θ_r is the sensor zenith angle, and $\vec{f_r}$ is the spectro-polarimetric BRDF at a given source / detector location. This assumes that the material is isotropic, thus allowing for '$\Delta\phi$' to be used.

$$\vec{L}_d = \tau_2(\theta_r) \iint_{\Omega_i} \vec{f_r}(\theta_i, \theta_r, \Delta\phi)\ cos\theta_i\ \vec{L}_d^{\Omega_i}(\theta_i, \phi)\ d\Omega_i \tag{7}$$

where $\vec{L}_d$ is the reflected downwelling sky radiance and $\vec{L}_d^{\Omega_i}(\theta_i, \phi)$ is the downwelling polarized radiance from a particular direction in the skydome hemisphere.

The upwelled radiance term,

$$\vec{L}_u = \vec{L}_u(\theta_r, \phi_r) \tag{8}$$

can be predicted along the reflected path from the scene to the imaging system using MODTRAN-p. This value will be assumed to be negligible since the current collection geometry has a relatively short sensor / target path length compared to airborne collections. The collection geometry will be explained in greater detail in section 3.2.

It should be noted that care must be taken when calculating the incident and reflected angles for use with the p-BRDF as in general this function is calculated with respect to the surface normal. In the case where the sample has no rotation, tilt, or spin relative to the global world coordinates no translations need to be calculated. Otherwise a rotation from global to local coordinates must be performed.

When considering non-diffuse materials, the downwelling term becomes a difficult parameter to estimate. This is because in order to estimate the integral, both the full 3x3 f_r matrix and the downwelling radiance must be known well enough to be sampled appropriately over the hemisphere. The hemispherical sampling resolution depends on both the structure of the downwelling radiance field, which is dependent on the current atmospheric conditions, and the BRDF structure which is dependent on the current material properties.

To isolate the downwelling term empirically, a modified version of the empirical line method (ELM) can be employed. The first step is to place multiple diffuse reflectance panels in the scene which have already been characterized. Each panel is oriented at a different angle relative to the primary source, which in this case is the sun. This will provide for different intensity values due to the cosine term in equation 6. A linear regression can then be performed relating the observed radiance L_s to $cos(\theta_i)$ to determine what will be termed the 'illumination' parameters of equation 6. To explain this process we revisit the governing equation for short sensing paths and will recast it into a linear form.

$$\begin{aligned}
\vec{L}s_{\theta_i} &= \vec{L}_r + \vec{L}_d \\
\vec{L}s_{\theta_i} &= \tau_1\ \tau_2\ E_s cos\theta_i \begin{bmatrix} f_{00} \\ f_{10} \\ f_{20} \end{bmatrix} + \tau_2 \iint_{\Omega} \vec{f_r}(\theta_i, \theta_r, \phi)\ cos\theta_i\ \vec{L}_d(\theta_i, \phi)\ d\Omega
\end{aligned} \tag{9}$$

Since we are assuming a diffuse randomly polarizing calibration panel, the above equation can be simplified into the linear form shown in equation 10.

$$\begin{aligned}
Ls_{\theta_i} &= \tau_1\ \tau_2\ E_s\ cos\theta_i\ \frac{r_d}{\pi} + \tau_2\ \frac{r_d}{\pi}\ L_d \\
&= \alpha\ cos\theta_i\ \frac{r_d}{\pi} + \tau_2\ \frac{r_d}{\pi}\ L_d \\
&= m\ cos\theta_i + B
\end{aligned} \tag{10}$$

The value for the slope term (m) and the diffuse reflectance of the panel (r_d) can then be used to solve for the 'illumination' term (α) which contains information about the atmospheric transmission and the exoatmospheric irradiance. Note that this assumes that the B term is constant for each angular location in θ_i. This assumption

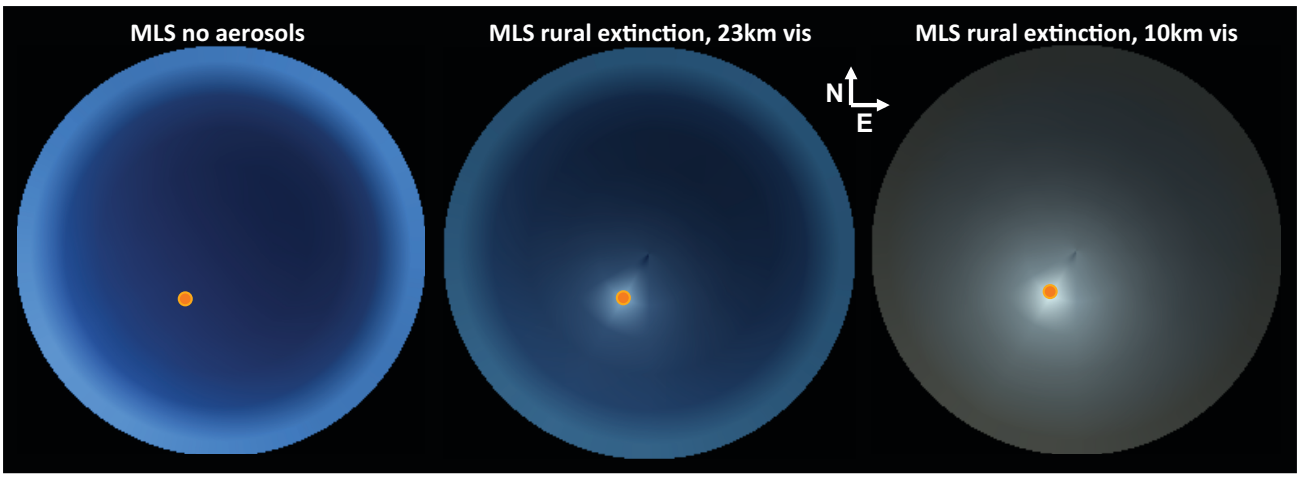

Figure 2. Modeled downwelling radiance using the MODTRAN atmospheric database for a typical collection time of 12:30pm utilizing different atmospheric assumptions. Orange dot represents approximate location of sun.

will require appropriate panel placement to take advantage of the symmetry present in the downwelling sky hemisphere. Figure 2 shows a model of this distribution for different atmospheric assumptions.

The α term, as well as the transmitted downwelling, can now be solved for by simply dividing the slope by the diffuse reflectance, shown in equations 11 and 12.

$$\alpha = \frac{\pi m}{r_d} \tag{11}$$

$$\tau_2 L_d = \frac{\pi B}{r_d} \tag{12}$$

The intercept term, B, contains information about the downwelling radiance as well as background and adjacency effects. However, since a diffuse panel is used, information about the polarimetric nature of the downwelling radiance is lost due to multiple internal scattering at the surface interface. This shortcoming can be overcome by placing a second pyramidal target panel that is not totally diffuse and will retain a polarimetric signature. It is proposed that the glossy panel can be assumed to have a p-BRDF that is made up of an un-polarized Lambertian scattering term and a polarized micro-facet based specular scattering term as seen in equation 13.

$$\begin{aligned} f(\theta_i, \theta_r, \Delta\phi) &= f_d + f_s(\theta_i^{spec}, \theta_s^{spec}, \Delta\phi^{spec}) \\ &= f_d + R_{gl}(-\gamma)\frac{P(\theta_n)F(\alpha)}{4cos(\theta_i)cos(\theta_r)}R_{gl}(\gamma) \end{aligned} \tag{13}$$

where γ is the angle of the target surface horizon with the global camera horizon, α is the local incident and reflection angle from the micro-facet that specularly scatters from the incident to reflected direction, θ_n is the angle of the micro-facet normal from the macro-facet normal, $P(\theta_n)$ is the probability of finding a micro-facet with that particular normal on the surface, $F(\alpha)$ is the Fresnel reflectance Mueller matrix, and R_{gl} is the rotation matrix for translating the stokes parameters from the global to the local reference frame (required for surfaces that are not flat to the ground plane).

Given this new version of the p-BRDF, the governing equation can now be expressed as a diffuse term and a specular term, shown in equation 14. Note the equivalence of the f_{01} and f_{10} terms that arises from the Fresnel Mueller matrix under the ideal specular scattering geometry.

$$\vec{L}_s = f_d\tau_2\left[E_s cos(\theta_i)\tau_1 + E_{sky}\right] + \tau_2 cos(\theta_{sky}) R_{gl}(-\gamma) f_s(\theta_i^{spec}, \theta_s^{spec}, \Delta\phi^{spec}) R_{gl}(\gamma)\Omega_s L_{sky}(\theta_i, \phi_i)$$

$$\begin{bmatrix} L_0 \\ L_1 \\ L_2 \end{bmatrix}_s = \begin{bmatrix} f_d\tau_2\left[E_s cos(\theta_i)\tau_1 + E_{sky}\right] \\ 0 \\ 0 \end{bmatrix} + \tau_2 cos(\theta_{sky}) R_{gl}(-\gamma) \begin{bmatrix} a & b & 0 \\ b & a & 0 \\ 0 & 0 & c \end{bmatrix} R_{gl}(\gamma)\Omega_s \begin{bmatrix} L_0 \\ L_1 \\ L_2 \end{bmatrix}_{sky}^{\theta_i,\phi_i} \tag{14}$$

The solid angle of the specular lobe (Ω_s) combined with the p-BRDF (f_s) can now be extracted by using several pieces of information. The rotation matrices $R_{lg}(\pm\gamma)$ are known by using scene geometry. The radiometric and atmospheric quantities of E_s, E_{sky}, $L_{sky}(\theta_i, \phi_i)$, τ_1, and τ_2 can be modeled with MODTRAN-P. The diffuse portion of the p-BRDF can be found by using the empirically derived values of α and $\tau_2 L_d$, shown in equation 15.

$$\begin{aligned} L_s &= \alpha\frac{r_d}{\pi} cos(\theta_i) + \frac{r_d}{\pi}\tau_2 L_d \\ L_s &= \frac{r_d}{\pi}(\alpha cos(\theta_i) + \tau_2 L_d) \\ f_d &= \frac{L_s}{(\alpha cos(\theta_i) + \tau_2 L_d)\pi} \end{aligned} \tag{15}$$

This equation also uses the assumption that the polarized specular portion of the BRDF is spectrally flat. This allows for the system to be over-determined and for a non-linear least squares approach to be used to solve for $\Omega_s f_s$, given enough spectral bands. Constraining $a \geq b$, $a \geq c$ and $c < 0$ produced the best results and conforms with the theoretical constraints of the Fresnel reflection Mueller matrix.[4] Figure 3 illustrates visually that the assumption of a spectrally flat polarized glint is a good one while section 4.2 will provide a more quantitative verification.

(a) Image of glossy green and black paint samples.

(b) Image with glare blocked by linear polarization filter.

Figure 3. Images taken of two glossy paint samples. The glint from the surface makes each sample appear to be the same color. If the glint is blocked with a polarizing filter, the true color of each sample can be seen.

When using this approach with spectro-polarimetric imagers it is not necessary to have the system calibrated radiometrically. The measured digital count values can be brought into modeled radiance space by comparing the modeled radiance to the measured DC of the diffuse panel. Equation 16 shows how a simple calibration coefficent can be found.

$$cc = \frac{L_{panel}}{DC_{panel} - DC_{dark}} \tag{16}$$

Ultimately, by using this approach, estimates for both the unpolarized diffuse (f_d) and the polarized specular (f_s) BRDF can be obtained for many glossy painted surfaces in the scene.

3. EXPERIMENTAL VALIDATION

3.1 Spectro-Polarimetric Imager (SPI)

The spectro-polarimetric imagery collected in this research was captured using a system that was custom integrated using commercial off the shelf components. Imagery is acquired using a GC780 gigabit ethernet CCD camera from Prosilica with a 35mm compact fixed focal length lens from Edmund Optics. This CCD array captures imagery monochromatically with a resolution of 782x582 and a pixel pitch of 8.3um square. The lens was chosen to allow for an angular FOV of 5.29° that will meet the acceptance angle specification of 7.5° for the liquid crystal tunable filter (LCTF). The LCTF is a 35mm VariSpec^{TM} from Cambridge Research & Instrumentation, Inc. (CRi) which allows for a very fast (5ms) adjustment of the 7nm bandpass from 400-720nm. The filter also acts as a linear polarizer and is attached to a rotation stage which allows for stokes parameters to be generated from imagery. This stage is computer controlled via serial connection to an Oriel controller. This allows for the LCTF to be actuated to different angular orientations thus allowing for the spectral stokes parameters to be determined. The entire system is attached to an optics bread-board base and can be placed on a tripod type mount which allows for different viewing geometries. Figure 4 shows the system attached to the tripod mount.

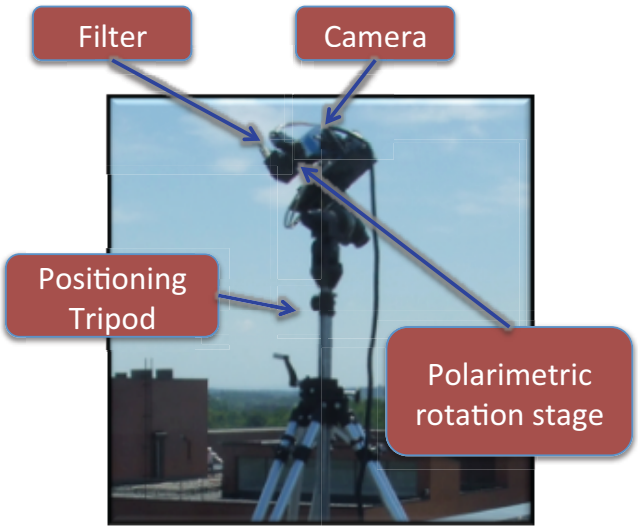

Figure 4. SPI system in use during an outdoor collection on a rooftop at the Rochester Institute of Technology (RIT). The system can be tipped or tilted to produce various viewing geometries.

When capturing spectro-polarimetric imagery outdoors, a balance must be found between maximizing the signal and minimizing the time between each polarimtric image set. The SPI system does this by coordinating the camera capture, the filter tuning, and the filter rotation motion using a custom control system developed in Labview. The integration time was decreased until the time between each polarimetric set was limited by the speed of the rotation stage. In an outdoor setting, close to noon, the optimal integration time was found to be around 100ms per image per band. The SPI captures four image sets at the following angles relative to the horizon: 0°,45°,90°,135°. A stokes vector can then be found using a modified Pickering Method[5] as given in equation 17

$$\begin{aligned} S_0 &= \frac{(E_0 + E_{45} + E_{90} + E_{135})}{2} \\ S_1 &= E_0 - E_{90} \\ S_2 &= E_{45} - E_{135} \end{aligned} \tag{17}$$

3.2 Scene Geometry

To test the retrieval process for both f_d and f_s, an experimental scene was designed outdoors. The scene location of a rooftop on the RIT campus was chosen initially as a location that has a simplistic background.

This assumption turned out to be less than ideal as will be shown in the results section, however many important lessons were learned for future field campaigns. As alluded to in the theory section, several calibration panels are needed to obtain the necessary information. The approach taken was to attach four panels to each side of a simple box. Each panel was hinged to one side of the box, and was supported by sliding angle brackets which allowed for each panel to be set at a specific angle with respect to the horizon. The box was then placed 22.6 ft to the east and 16.75 ft below of the SPI. This viewing distance was chosen to both fit the panels in the FOV while still placing a reasonable number of pixels on each panel. Figure 5 shows this setup. Each panel was broken into 6 different regions, each of which had a different type of paint. The colors from the left to the right are black, green, and white. The top row is a diffuse 'matte' type while the bottom row is of a specular 'glossy' type. This will allow for the extraction of the polarimetric specular lobe from the glossy row using the diffuse row as a calibration material.

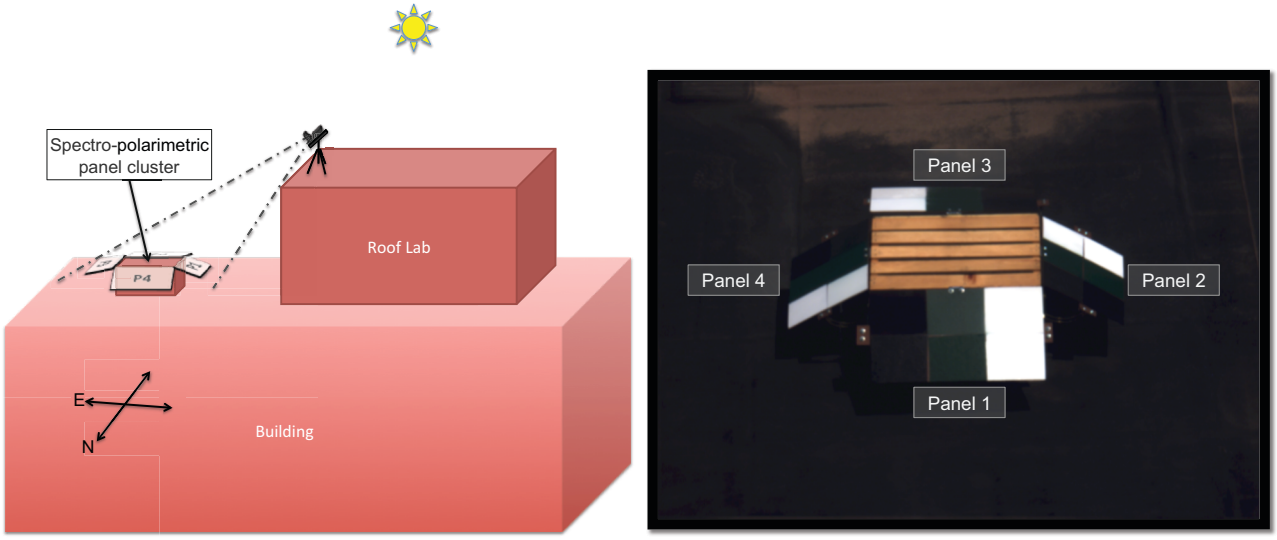

(a) Scene geometry (b) RGB composite of panel cluster as seen from the SPI

Figure 5. The SPI was placed above and to the west of the polarimetric calibration panel cluster.

The (x,y,z) locations of the panel cluster and the SPI were found using differential GPS processing with the GeoXT from Trimble. The SPI was tilted to give a $\theta_s = 51°$. The collection was performed at 13:52 yielding a sun location of $\theta_i = 21.3°$ and $\phi_i = 205.3°$. Table 1 shows the source and zenith angles in local coordinates relative to each panel surface normal along with the predicted percent change in solar irradiance due to the cosine effect.

Table 1. Local panel coordinates and cosine law effect.

Panel	Sun Zenith (θ_i^{loc})	SPI Zenith (θ_s^{loc})	Delta Azimuth ($\Delta\phi^{loc}$)	$cos(\theta_i)$
1	29.561	18.600	138.266	0.870
2	15.551	57.824	-31.276	0.963
3	36.656	73.400	33.373	0.802
4	51.969	57.745	55.408	0.616

3.3 Laboratory Characterization

Each paint was also applied to a smaller sample square of panel material and characterized using a Cary 500 FTIR Spectrophotometer by Varian. This machine has the capability of measuring the total diffuse hemispherical reflectance including the specular lobe. It is also possible to configure the measurement to trap the specular component and measure just the diffuse portion of the hemispherical reflectance. This allows for the hemispherical f_s component to be determined spectrally for the glossy samples.

3.4 Synthetic Scene Generation: DIRSIG

The scene was also modeled using the Digital Imaging and Remote Sensing Image Generation Model[5] (DIRSIG) software model. DIRSIG inherently performs all radiometric calculations spectrally with Stokes vectors and Mueller matricies. Leveraging MODTRAN-P to model the solar and sky radiance, as well as attributing polarimetric BRDF properties to object surfaces, results in a spectrally resolved, aperture reaching Stokes vector radiance. The skydome radiance is precomputed before running the DIRSIG scene model to generate a spectrally resolved atmospheric database of exoatmospheric solar irradiance, sun to target transmission, target to camera path radiance, and polarized sky radiance sampled at 6 zenith and 12 azimuthal directions (for a total of 72 sky samples). Figure 6 shows the CAD model (generated in the open source software program Blender) of the calibration panel cluster along with a RGB rendering of the S0 polarimetric state. The S1 and S2 states are also shown for the 554 nm band.

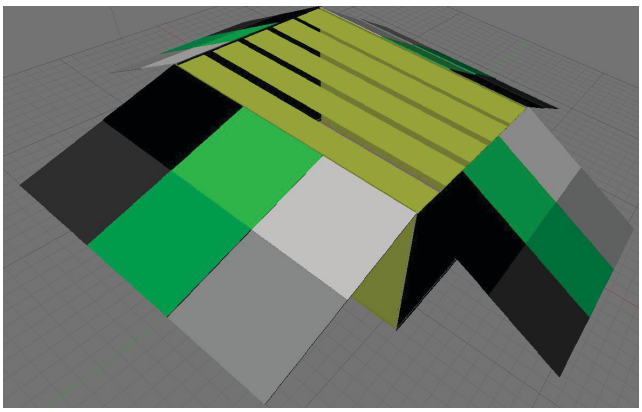

(a) CAD model of panel cluster created using the Blender software package.

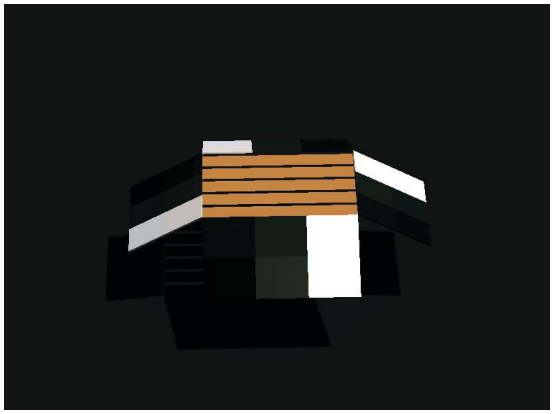

(b) Simple scene rendered using DIRSIG.

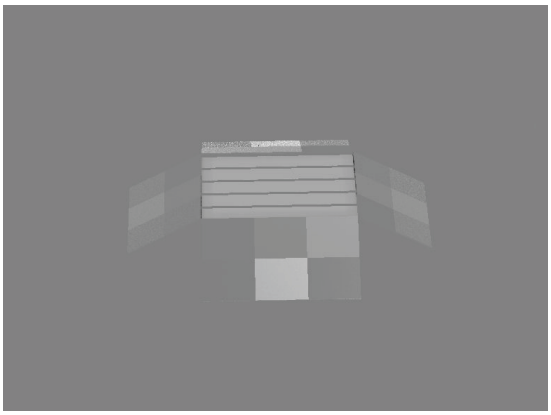

(c) DIRSIG S1 image of scene at 554 nm.

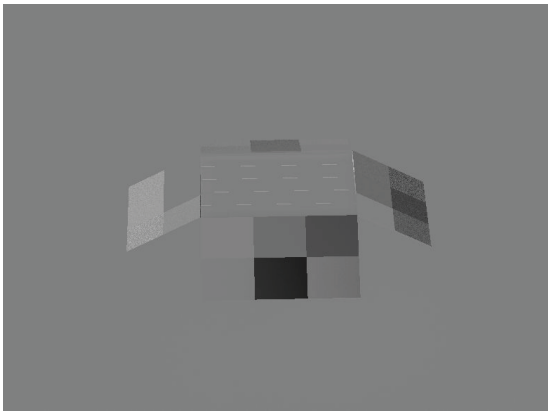

(d) DIRSIG S2 image of scene at 554 nm.

Figure 6. Various portions of the DIRSIG scene created.

4. RESULTS

The approach to retrieve the diffuse and specular components of the p-BRDF (f_d and f_s) using equation 14 was applied to the white sections of the panel cluster, in that they provided the largest signal in the measured data. The retrieval was attempted on the green and black panels, but the limited dynamic range (8-bit) of the raw imagery kept these panel signatures down in the noise. In particular, the north and south facing panels (panels 2 and 4) were used because they provide the greatest contrast in signal as predicted in table 1. The specular component for the p-BRDF was retrieved from the north facing panel for reasons which will be

discussed in section 4.2. The specular component of the p-BRDF was found for a incident/scattered geometry of $(55°, 55°, 180°)$. Coincidentally, this scattering angle was close to the Brewster angle for the paint resulting in excellent polarimetric contrast. This convention was followed when using the simulated data as well.

4.1 Radiometric Model

The simulated sensor reaching radiance for the north facing panel was extracted from the simulated imagery, as seen in figure 6(b), by a user defined region of interest (ROI) and used in the retrieval process. The diffuse portion of the white glossy panel in this case does not need to be solved for by equation 15 since it is a known when creating the model. We would expect a perfect retrieval in this case since the modeled data is noise-free. However, as seen in Figure 7, there is a small amount of residual error. This is because the sky sampled by the glossy specular lobe does not fall directly on the samples chosen by the DIRSIG simulation so some linear interpolation occurs resulting in the small residual error.

(a) Glossy white ROI from DIRSIG scene.

DIRSIG Surface Optical Property Truth

$$f_s(55°, 55°, 180°)\Omega_s = \begin{bmatrix} 0.092 & 0.09 & 0 \\ 0.09 & 0.092 & 0 \\ 0 & 0 & -0.012 \end{bmatrix}$$

Value derived from analysis of DIRSIG scene

$$f_s(55°, 55°, 180°)\Omega_s = \begin{bmatrix} 0.089 & 0.089 & 0 \\ 0.089 & 0.089 & 0 \\ 0 & 0 & -0.013 \end{bmatrix}$$

Retrieval Error

$$Error = \begin{bmatrix} 0.003 & 0.001 & 0 \\ 0.001 & 0.003 & 0 \\ 0 & 0 & 0.001 \end{bmatrix}$$

(b) Specular p-BRDF retrieval results using synthetic data.

Figure 7. Results from retrieving the specular p-BRDF from simulated scene data.

4.2 Real Data

The same approach was taken using the data collected with the SPI system. In this case, the diffuse portion of the glossy white sample was retrieved by utilizing the matte white sample to solve for the α and $\tau_2 L_d$ terms in equations 11 and 12. Equation 15 can then be used to solve for the diffuse portion of the glossy white panel. This approach requires the a-priori knowledge of r_d for the matte sample. Therefore the hemispherical reflectance was measured in the lab for the matte white sample. The glossy white material was also measured to test the assumption that the specular reflectance is spectrally flat. The results for this measurement are shown in Figure 8. As can be seen, the specular reflectance of the glossy paint is spectrally flat which has an average specular reflectance of $3.49\% \pm 0.039\%$ across the spectral range sampled.

The measured digital counts were then moved into modeled radiance space by again using the matte white panel. Equation 16 was calculated by using the average DC and the average modeled radiance from DIRSIG of the panel. The data also had noise present which was most noticable in the S1 and S2 bands. To obtain a better signal-to-noise ratio, the measured data was spectrally up-sampled from 7nm to 49nm bandpasses. This allowed for much greater signal while still retaining enough known inputs to allow for a solution to converge in equation 15 which was then calculated for the white glossy paint for panel 3. Panel 3 was chosen since it had the least amount of background effects and the clearest view of the sky. Figure 9 explains issues present for each panel as well as presents the retrieved diffuse term for the glossy white panel.

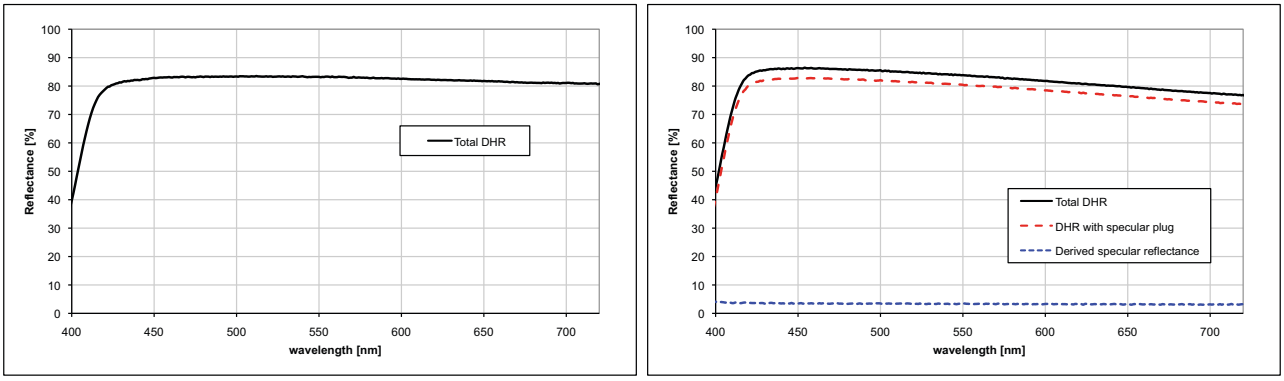

(a) DHR for matte white paint. (b) DHR for glossy white paint.

Figure 8. Laboratory measured DHR for white paints. Glossy sample measured with and without specular plug.

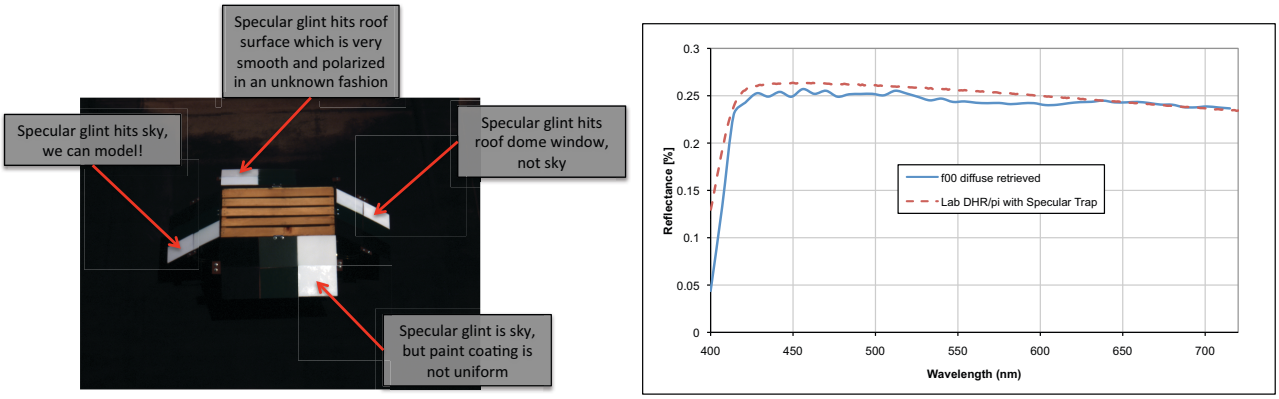

(a) Background effects present for each panel. (b) Retrieved f_d versus laboratory measured.

Figure 9. Each panel with the exception of panel three was rejected from analysis, shown in (a). The retrieved f_d matches well with laboratory measured f_d. Signal begins to drop in the blue due to system sensitivity as the wavelength approaches 400nm.

In order to assess the accuracy of the retrieved f_s term, a model was created using the expected Fresnel reflectance from an average plastic material. The index of refraction of plastics are commonly real valued (dielectric) and may vary between 1.5 and 1.6. For our comparison, we chose an arbitrary value of 1.55 since we do not know the exact polymer used in the paint to create the glossy finish. Figure 10 shows the predicted vertical and horizontal reflectance over the range of reflected view angles as well as a comparison between the predicted f_s term versus the retrieved for this experiment's specific geometry.

These results show that it is possible to retrieve the diffuse f_d BRDF on a spectral basis as well as the polarized specular f_s matrix for a specific geometry using field data. The sensed digital counts were transfered into modeled radiance units using the white diffuse panel which allowed for the empirical calibration of the SPI. While these results are promising, a more robust method of handing background influences is needed.

5. CONCLUSIONS

A process is proposed to break the p-BRDF for glossy specular materials into diffuse and specular components. The diffuse component is solved for by using a-priori knowledge for the BRDF of a separate lambertian material which is oriented with at least two different relative source zenith locations. Several additional radiometric and atmospheric terms are then modeled using MODTRAN-P. Using a non-linear least squares approach and the sensor reaching Stokes parameters, the specular component of the p-BRDF coupled with the solid angle subtended by the glossy specular lobe can be retrieved. This value can be used as a good indication of how strong the material may appear in polarimetric terms. More specifically, this information can be used to model

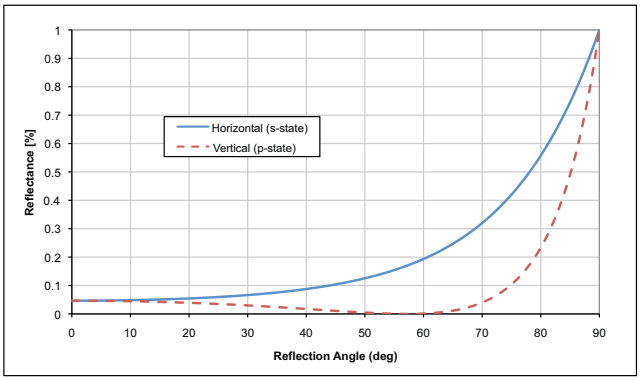

(a) Predicted reflectance using Fresnel theory.

Fresnel Theory Prediction

$$f_s(55°, 55°, 180°)\Omega_s = \begin{bmatrix} 0.081 & 0.081 & 0 \\ 0.081 & 0.081 & 0 \\ 0 & 0 & -0.005 \end{bmatrix}$$

Value derived from analysis of field imagery

$$f_s(55°, 55°, 180°)\Omega_s = \begin{bmatrix} 0.086 & 0.086 & 0 \\ 0.086 & 0.086 & 0 \\ 0 & 0 & -0.000 \end{bmatrix}$$

Retrieval Error

$$Error = \begin{bmatrix} 0.005 & 0.005 & 0 \\ 0.005 & 0.005 & 0 \\ 0 & 0 & 0.005 \end{bmatrix}$$

(b) Specular p-BRDF retrieval results using real data.

Figure 10. Results from retrieving the specular p-BRDF from field data.

the polarimetric contrast of the target with different backgrounds and in scenes with various clutter contents and object geometries. Such information could in the future lead to the development of improved algorithmic performance for applications such as target detection as well as optimization of asset tasking. This process could also be implemented in denied areas using in-scene materials in place of the calibration panel cluster. For example, in an arid environment, sand dunes could be used as a randomly polarizing diffuse material that also has multiple angles. Further work to evaluate the feasibility of such an approach is needed.

The collection performed using the spectro-polarimetric imager (SPI) shows the importance of background influences on polarimetric objects within a scene. Since this approach relies on tilting the calibration materials, it is of critical importance to assess the polarimetric nature of the background. In this case, the smooth roof surface surrounding the calibration materials was highly polarized which was difficult to model. Further work for including the background effects on glossy materials in the modeling process is needed.

REFERENCES

[1] Harmel, T. and Chami, M., "Invariance of polarized reflectance measured atthe top of atmosphere by parasol satelliteinstrument in the visible range with marineconstituents in open ocean waters," *Opt. Express* **16**(9), 6064–6080 (2008).

[2] Walraven, R., "Polarization imagery," *Optical Polarimetry: Instrumentation and Applications* **112**, 164–167, SPIE (1977).

[3] Shell, J. R. and Schott, J. R., "A polarized clutter measurement technique based on the governing equation for polarimetric remote sensing in the visible to near infrared," *Targets and Backgrounds XI: Characterization and Representation* **5811**(1), 34–45, SPIE (2005).

[4] Kattawar and Adams, "Stokes vector calculations of the submarine light field in an atmosphere-ocean with scattering according to a rayleigh phase matrix: effect of interface refractive index on radiance and polarization," *Limnol. Oceanogr.* (34), 1453–1472 (1989).

[5] Schott, J. R., [*Fundamentals of Polarimetric Remote Sensing*], vol. TT81, SPIE Tutorial Texts In Optical Engineering (2009).